PCCP

PAPER

View Article Online
View Journal | View Issue

Cite this: *Phys. Chem. Chem. Phys.*, 2014, **16**, 12341

"Ionic liquids-in-salt" – a promising electrolyte concept for high-temperature lithium batteries?

Maciej J. Marczewski,*[a] Bernhard Stanje,[b] Ilie Hanzu,[bc] Martin Wilkening[b] and Patrik Johansson*[ac]

Received 17th March 2014,
Accepted 28th April 2014

DOI: 10.1039/c4cp01133c

www.rsc.org/pccp

A novel electrolyte concept for lithium-ion batteries, termed "ionic liquid-in-salt", is introduced. Our feasibility study on $(1-x)$EMIMTFSI:(x)LiTFSI, $0.66 \leq x \leq 0.97$, showed that at elevated temperatures the various dual liquid and solid phase regions are characterized by a wide thermal stability window, high ionic conductivities and appreciable mechanical integrity. The highest conductivity values are obtained for the compositions $x = 0.70$ and $x = 0.75$ ($\sigma \approx 6 \times 10^{-3}$ S cm^{-1}) and are related to the final melting of the materials. Overall, high conductivities are observed for $0.70 < x < 0.90$ while low ones are found for $x > 0.90$. Raman and NMR spectroscopies reveal the presence of highly mobile Li-containing species, partly identified as $[Li(TFSI)_2]^-$, albeit rather unexpected for these high x values, which might explain the high ionic conductivities observed. To prove the general value of our concept in more detail, some first results on BMIMTFSI and PY_{13}TFSI based systems are also presented.

1 Introduction

The last two decades have been the time of the omnipresent commercialization of rechargeable lithium-ion batteries. However, today's lithium-ion battery technology is a compromise between high performance and safety, with serious safety issues originating from electrolytes based on the metastable $LiPF_6$ salt that demands stabilizing additives, and organic solvents, which are prone both to decompose and to inflame.[1] Especially for larger batteries, aimed at application in electric or hybrid electric vehicles as well as for load-levelling, intrinsically safer batteries, preferably based on thermally and electrochemically stable electrolytes with high ionic conductivities, *i.e.*, excellent ion transport properties, are urgently needed. One possibility to improve existing lithium-ion batteries is to develop electrolytes based on ionic liquids (ILs).[2,3] There are many groups developing and testing electrolytes based on ILs doped with lithium salts, LiX, with X being any anion. Most common are binary systems, $IL_{(1-x)}$–LiX_x, but ternary systems have also been thoroughly studied.[4–6] The focus has so far been on systems with low or medium LiX concentrations, $0.01 < x < 0.5$, ("LiX-in-IL"), but a few papers report on systems with $x > 0.5$, up to 0.7 or even 0.8, systems for which we here coin the term "ionic liquid-in-salt" or specifically "IL-in-LiX".[7,8] Another possible answer to the challenge of battery safety is to use electrolytes intrinsically designed for use at elevated or even at very high temperatures. These are often based on solid polymer electrolytes or molten salts[9–11] but here the potential of IL based electrolytes has also been recognized.[12]

Here, we combine the two notions by presenting high temperature studies (up to 180 °C) on "ionic liquid-in-salt" systems with large amounts of lithium salt ($x \geq 0.66$) being in analogy with the "polymer-in-salt" and the very recent "solvent-in-salt" concepts.[13,14] Until now, systems with $x \geq 0.66$ have not attracted any interest due to their very low ionic conductivities, low Li transference numbers at room and moderate temperatures as well as because of the poor reproducibility of the results obtained. This might change when they are used at elevated or high temperatures (*ca.* 90 °C to 120 °C). "IL-in-salts" may become promising as intrinsically safe, thermally and electrochemically stable electrolytes with both high ionic conductivities and appreciable mechanical properties.

For this proof-of-concept study of "IL-in-LiX" systems it is important to use a simple but also relevant model system. The IL should be characterized by high thermal stability, high ionic conductivity, and it should possess the same anion as the lithium salt. The lithium salt should be thermally stable as well. Furthermore, it should be able to form homogenous melts or solutions in organic solvents being compatible with the IL and the preparation method chosen. To enable a more complete study, knowledge about the entire possible phase behaviour of the IL and LiX is of importance; hence, a previously well-studied "LiX-in-IL" system should preferably be selected. The reason for the latter is that local heterogeneities may occur, due to

[a] *Department of Applied Physics, Chalmers University of Technology, SE-41296, Göteborg, Sweden. E-mail: m_marczewski@ch.pw.edu.pl, patrik.johansson@chalmers.se*
[b] *Christian Doppler Laboratory for Lithium Batteries, Institute of Chemistry and Technology of Materials, Graz University of Technology, 8010 Graz, Austria*
[c] *ALISTORE-ERI European Research Institute, 33 rue Saint Leu, 80039 Amiens, France*

preparation, cooling, and storage conditions, or even during employment inside an electrochemical cell. Thus, any phase which can potentially be formed is relevant, not only those being thermodynamically stable. Furthermore, to make the system more predictable, as few phases as possible within the temperature range, defined by the working temperature (*ca.* 90 °C) and room-temperature storage conditions (*ca.* 20 °C), are preferred.

With the above considerations applied, the IL and LiX pair selected is 1-ethyl-3-methyl-imidazolium bis(trifluoromethanesulfonyl)imide (EMIMTFSI) and the corresponding LiTFSI lithium salt. These together create the model system $(1 - x)$EMIMTFSI:(x)LiTFSI, or shorter $Li_xEMIM_{(1-x)}TFSI$. Crystalline phases form for $x < 0.25$ (solid EMIMTFSI) and for the composition with $x = 0.67$ (1 : 2 EMIMTFSI/LiTFSI crystal) whereas between $0.25 < x < 0.55$ this system is fully amorphous at room-temperature.[8,15,16] For other x variations and temperatures, however, the system exists in different double phase regions – each with its own characteristics of, for example, ionic conductivity and other properties relevant for practical battery electrolyte usage, such as mechanical strength and Al corrosion propensity.

To strengthen the fundamental understanding of this new concept, giving promise to further rational improvement, we also aim to arrive at a congruent picture of the structure–property relationship of these new electrolytes. This is done by connecting the macroscopic property performance observations with the molecular level origin in terms of local ion coordination, charge carrier concentration, anion conformation, mobility and diffusivity *etc.* For the latter there is indeed a wide bibliography of both calculated and measured NMR, IR and Raman spectra for EMIMTFSI and LiTFSI individually and for the "LiX-in-IL" systems.[17–23] Furthermore, to show the generality of the concept proposed, the $Li_xBMIM_{(1-x)}TFSI$ and $Li_xPY_{13(1-x)}TFSI$ systems are also presented.

2 Experimental section

Materials

1-Ethyl-3-methylimidazolium bis(trifluoromethanesulfonyl)imide, EMIMTFSI (purity 99.9%), 1-butyl-3-methylimidazolium bis(trifluoromethanesulfonyl)imide, BMIMTFSI (purity 99.9%) and *N*-propyl-*N*-methylpyrrolidinium bis(trifluoromethanesulfonyl)imide, $PY_{13}TFSI$ (purity 99.9%) were all purchased from Solvionic and used as received. In all cases the water amount was <30 ppm as determined by Karl Fischer titration. Lithium bis(trifluoromethanesulfonyl)imide, LiTFSI (purity 99.95%), was purchased from Sigma Aldrich and dried under vacuum for 72 h at 80 °C before use. All materials were stored in an argon filled glove box ($H_2O < 1$ ppm, $O_2 < 1$ ppm).

Sample preparation

The samples were prepared in an argon filled glove-box, *i.e.*, under inert conditions. Materials were prepared by direct mixing of weighted appropriate quantities in glass tubes placed in an oven, heated to 250 °C and held at this temperature for 1 hour. After cooling to room temperature a spatula was used to homogenize the samples, thereafter the procedure was repeated but with a shorter heating time (30 min). This way, (i) a set of eight $(1 - x)$EMIMTFSI:(x)LiTFSI mixtures with $x = 0.66$, 0.70, 0.75, 0.80, 0.85, 0.90, 0.93, and 0.97, (ii) a set of three $(1 - x)$BMIMTFSI:(x)LiTFSI mixtures, $x = 0.70$, 0.80, and 0.90, and (iii) a set of five $(1 - x)PY_{13}TFSI$:(x)LiTFSI mixtures, $x = 0.75$, 0.80, 0.85, 0.90, and 0.96, were prepared.

Differential scanning calorimetry

Thermal data were obtained by measuring about 10 mg of the sample placed in aluminum hermetic pans using a TA Instrument Q1000 Differential Scanning Calorimeter (DSC). The DSC scans were performed as follows. After equilibration at 40 °C the samples were cooled down to −150 °C using a cooling rate of 5 °C min^{-1}. Subsequently, the samples were equilibrated at −150 °C for three minutes and thereafter heated to 250 °C at a heating rate of 5 °C min^{-1}. After 3 minutes of equilibration at 250 °C, the samples were cooled down to −150 °C using a cooling rate of 5 °C min^{-1} and equilibrated for at least 3 minutes. Finally, samples were heated from −150 °C to 250 °C at a rate of 5 °C min^{-1}. $(1 - x)$EMIMTFSI:(x)LiTFSI samples with $x = 0.66$, 0.70 and 0.75 were heated up to 160 °C and 200 °C respectively. For the $(1 - x)$BMIMTFSI:(x)LiTFSI samples only the first heating cycle was performed. Reported melting temperatures are peak temperatures.

Ionic conductivity measurements

The temperature dependence of the ionic conductivity was measured by dielectric spectroscopy using a Novocontrol broadband dielectric spectrometer at frequencies ranging from 10^{-1} to 10^7 Hz. The sample (about 0.3 g) was placed between two stainless steel electrodes with a Teflon spacer (13.2 mm in diameter and 0.99 mm in thickness) and loaded into a cryofurnace with nitrogen flow. The cell, "Liquid parallel plate cell BDS 1308" – Novocontrol, was assembled in an argon atmosphere. Data were collected during heating from 20 °C to 180 °C with a temperature step of 10 °C and a stabilization time of 30 min at each temperature. The DC conductivity was deduced from the low frequency plateau of the conductivity isotherms obtained by plotting the real part of the complex conductivity as a function of frequency.

Raman spectroscopy

FT-Raman spectra were recorded on a Bruker MultiRAM Stand-Alone FT-Raman Spectrometer using a Nd-YAG laser (1064 nm). Typically, the recording time for a single spectrum was 3 to 4 h. The laser power was in the range of 100 to 350 mW for all samples. Raman spectra were measured over the frequency range 0 to 3600 cm^{-1}. The spectra were normalized by integrating the intensity of the most intense Raman band between 720 and 780 cm^{-1}. For measurements at 90 °C and 165 °C, the samples were placed on a glass plate in a hermetically sealed Linkam FTIR600 temperature controlled stage filled with dry argon gas. Before the measurements, each sample was held at 90 °C (or 165 °C) for 40 min.

^{7}Li NMR measurements

^{7}Li NMR measurements were performed using a high-performance Bruker Avance III 500 MHz spectrometer which is permanently connected to a shimmed 11.7 T cryomagnet with a nominal ^{7}Li resonance frequency of 194.3 MHz. A commercial broadband probe (Bruker Biospin) was employed to measure temperature-variable ^{7}Li NMR line shapes under static, *i.e.*, non-rotating conditions. ^{7}Li NMR lines were acquired by applying a saturation recovery pulse sequence ($10 \times \pi/2 - t_d - \pi/2$ – acquisition). The initial pulse train, consisting of ten $\pi/2$ pulses, was used to destroy any longitudinal magnetization M_z. Immediately after, M_z recovers according to spin–lattice relaxation determined by the rate $1/T_1$. After a sufficiently long waiting period t_d, M_z was flipped with a $\pi/2$ pulse. In the rotating frame of reference, M_z decays due to spin–spin relaxation. Fourier transformation of the resulting free induction decay produces the spectra shown. Typically, the $\pi/2$ pulse lengths ranged between 2.60 and 3.20 μs, *i.e.*, the Li spins have been non-selectively excited. The WSolids software was used to estimate NMR coupling constants and asymmetry parameters.[24]

3 Results and discussion

Thermal behaviour

First, the thermal behaviour of all compositions was studied and overall found to be in very good agreement with previous reports.[5,7,8] Pure LiTFSI is characterized by a solid–solid transition at 152 °C and a melting temperature at approximately 234 °C (Fig. 1). Whereas the crystal structure of the low-temperature solid phase (IIa) has been previously well described,[25] that of the high temperature solid phase (Ia) is still not characterized. In Fig. 2a the corresponding temperature variable solid-state ^{7}Li NMR spectra are shown. The spectrum of the low temperature phase IIa is composed of a central line with a width (full width at half maximum) of approximately 3.6 kHz. Next to the central transition satellite intensities show up which are due to the interaction of the quadrupole moment of the ^{7}Li spin with an electric field gradient (EFG) at its site.[26] Note that ^{7}Li is a spin-3/2 quadrupole nucleus, *i.e.*, in addition to the interaction with the external magnetic field, the Zeeman levels are altered by electric quadrupolar interactions. In general, a non-vanishing EFG is produced by the electric charge distribution in the direct neighborhood of the ^{7}Li nucleus.[26,27] In LiTFSI the Li ions occupy a single crystallographic site. The NMR quadrupole powder pattern observed points to an EFG characterized by a quadrupole coupling constant C_q of approximately 50 kHz as estimated from the outer singularities whose position remains largely unaffected by the other NMR parameters influencing the overall spectrum. From the inner singularities in combination with a preliminary simulation we estimate the corresponding asymmetry parameter η of the EFG to be approximately 0.3. Note that the individual positions (and relative intensities) of all singularities (see the inset of Fig. 2a) with respect to the central line can be explained by taking into account a slight chemical anisotropy in combination with a proper choice of the corresponding Euler angles. The latter characterize the chemical shift tensor when going from the crystal frame to the principal axis system.

With increasing temperature C_q being characteristic for the EFG in the IIa phase of LiTFSI slightly increases which is most likely due to extremely small changes in the lattice parameters of this phase. The overall features of the NMR spectrum, however, remain untouched. At temperatures above

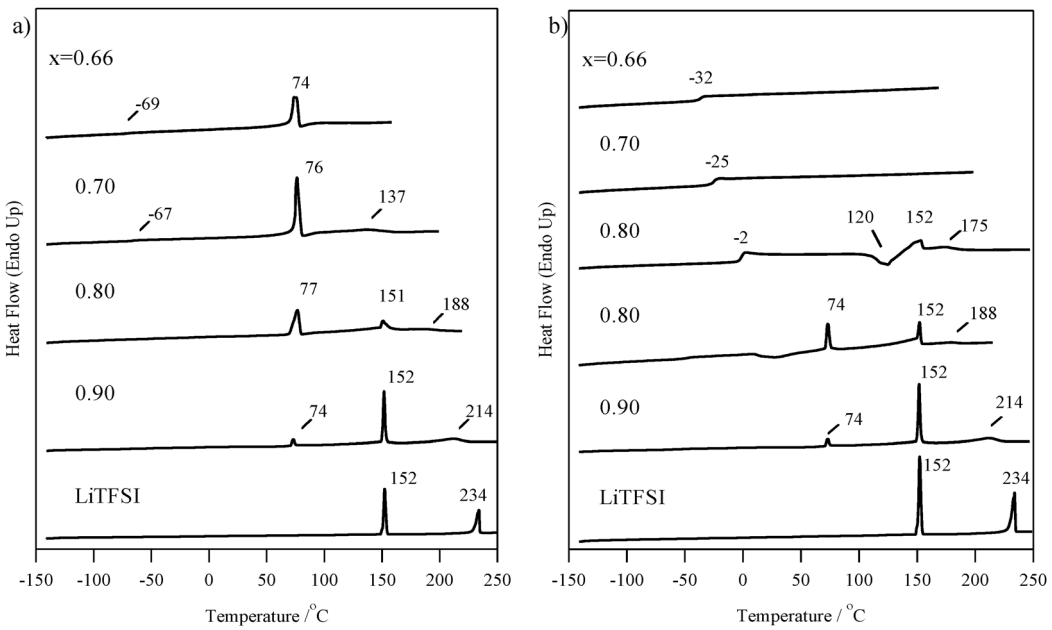

Fig. 1 DSC heating traces for the $Li_xEMIM_{(1-x)}TFSI$ ($0.66 \leq x \leq 1$) system; data collected during the first heating cycle (a), data collected during the second heating cycle (b).

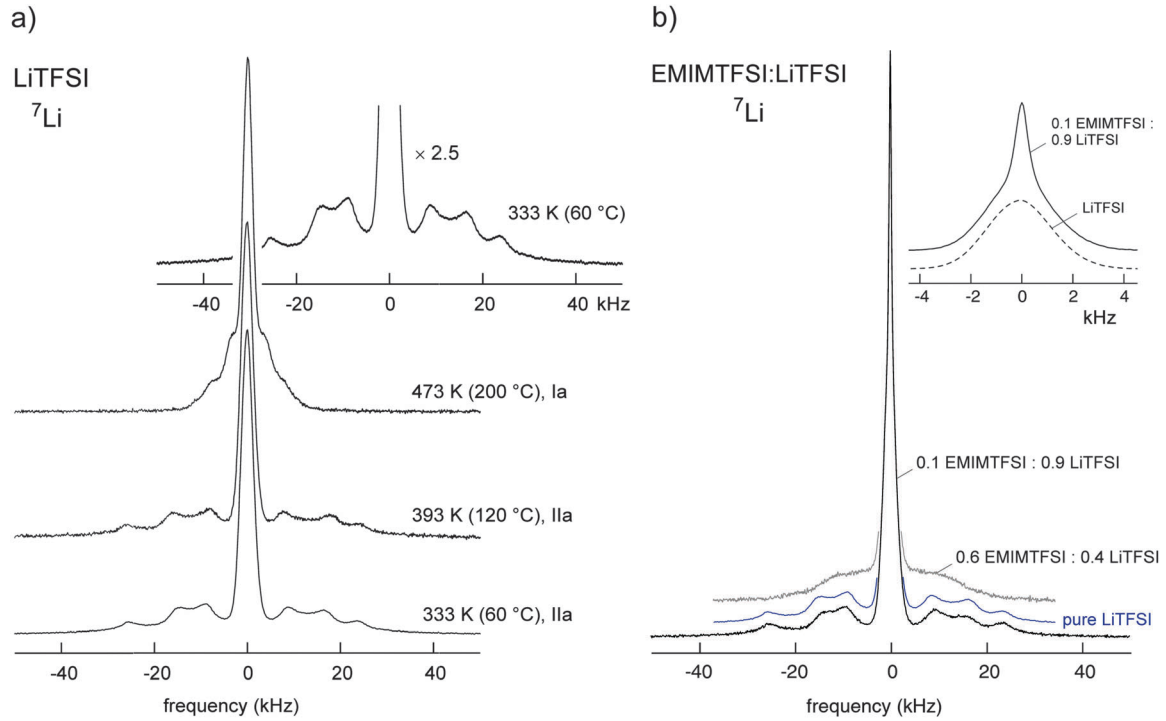

Fig. 2 Solid-state ^{7}Li NMR spectra (194.3 MHz) of pure crystalline LiTFSI recorded at the temperatures indicated, the inset shows a magnification of the quadrupole powder pattern of the spectrum recorded at 333 K (phase IIa). (a) The corresponding ^{7}Li NMR spectrum of $Li_xEMIM_{(1-x)}TFSI$ with x = 0.9; for comparison the quadrupole satellite intensities of the samples with x = 1 (pure LiTFSI) and x = 0.6 LiTFSI are also shown. (b) The inset illustrates the shape of the central NMR line of $Li_{0.9}EMIM_{0.1}TFSI$ being composed of two components reflecting fast and slow Li ions. The central line drawn with a dashed line represents that of pure LiTFSI. See the text for further explanation.

the solid–solid phase transition, a major change occurs and C_q of the newly formed Ia phase is reduced by more than a factor of 2 compared to its initial value in the IIa phase. This perfectly agrees with the DSC based observations.

For the as prepared mixed samples, doping of LiTFSI with EMIMTFSI ($0.66 < x < 1$) results in the formation of up to three dual phase regions before the samples finally melt (Fig. 1a).

Starting from low temperatures up to the phase transition at *ca.* 76 °C, a new double phase region is observed for $x > 0.66$, which can be attributed to crystalline 1/2 EMIMTFSI/LiTFSI (Ib) and solid LiTFSI (IIa). ^{7}Li NMR (Fig. 2b) reveals that the spectrum of a sample with x = 0.9 mainly resembles that of pure LiTFSI (IIa), particularly when the well-resolved quadrupole powder pattern is regarded. In contrast to pure LiTFSI, however, the central line is composed of two components (see inset of Fig. 2b). Whereas the broad one coincides with that of pure LiTFSI, the (motionally narrowed) NMR line on top can be attributed to Li ions being much more mobile than those in the IIa LiTFSI phase. In general, averaging of dipole–dipole interactions because of rapid diffusive motions of the Li spins causes narrowing of the dipolarly broadened ^{7}Li NMR lines. Significant narrowing is expected when the mean Li jump rate becomes larger than the spectral width of the NMR line at low temperatures. The latter is often called the *rigid lattice* line width. In the present case, the motionally narrowed NMR components point to exchange rates of the order of 10^3 s^{-1} at ambient temperature. Most importantly, the highly mobile ions do already show up at room temperature. They can be related to those forming the Ib phase with mixed cations. Since the overall conductivity is relatively low at ambient temperature (see below), the mobile ions might be involved in jump processes restricted to shorter length scales. Increasing the amount of EMIMTFSI further results in a quadrupole powder pattern being smeared out, indicating an increased structural disorder resulting in a broad distribution of EFGs (Fig. 2). Samples with $x > 0.7$ also show high ionic conductivities at room temperature (Fig. 5 and below).

In the literature the melting of the Ib phase was reported to occur at approximately 82 °C.[8] For $x \leq 0.70$ a small amount of an amorphous phase is also observed (with $T_g \approx -69$ °C). Between 76 °C and 151 °C another double phase region, obtained from melting of the 1/2 EMIMTFSI/LiTFSI phase is present which consists of liquid (0.33–0.25)EMIMTFSI:(0.67–0.75)LiTFSI (L) together with solid LiTFSI (IIa). The melting temperatures of samples with $0.70 < x < 0.75$ range from 137 °C to 151 °C. A high temperature liquid–solid double phase region is observed only for $x > 0.75$ and exists at temperatures between 151 °C and the final melting point. The melting point depends on overall composition x and ranges from *ca.* 153 °C up to 230 °C. The phase consists of liquid (0.25–0.03)EMIMTFSI:(0.75–0.97)LiTFSI (L) together with solid LiTFSI (Ia). Temperature variable ^{7}Li NMR spectra excellently agree with the structural changes outlined (Fig. 3). At low temperatures the quadrupole powder pattern stems from LiTFSI; with rising temperature the pattern changes and we observe the

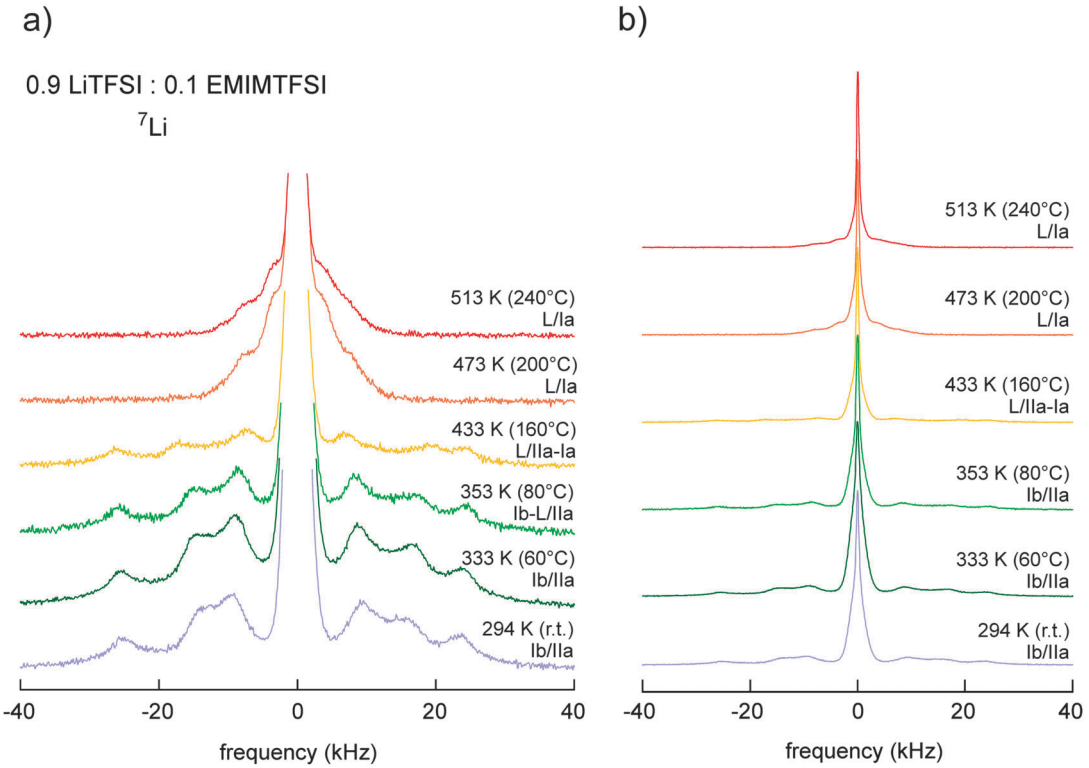

Fig. 3 Change in the solid-state ^{7}Li NMR spectra (194.3 MHz) of $Li_xEMIM_{(1-x)}TFSI$ with x = 0.9 with increasing temperature; (a) the lower part of the spectra magnifying the quadrupole powder pattern, (b) full spectra revealing the two-component NMR central transition. The area fractions of the two NMR lines (see also the inset of Fig. 2b) are plotted in Fig. 4 as a function of temperature.

solid–solid IIa–Ia phase transition. Interestingly, melting of the Ib phase seems to partly affect the pattern of the IIa phase of LiTFSI as can be seen when the spectrum recorded at 80 °C (and 160 °C) is considered. At 200 °C the formation of the Ia phase has been completed. The spectrum recorded at 240 °C still has non-vanishing satellite intensities present, a signature of the crystalline LiTFSI phase (Ia). In Fig. 3b the complete NMR spectra are shown focusing on the central lines. With increasing T the number fraction of mobile Li ions, directly reflected by the area fraction of the narrowed NMR line, increases from 20 to 30% (see Fig. 4), in perfect agreement with the results mentioned above. This increase is directly in line with the increase of the overall conductivity of the sample with x = 0.9 taking place between 30 and 70 °C which is below the melting point of the Ib phase (*cf.* Fig. 4 and 5). The correlation with the ionic conductivity indicates that the mobile ions seen by NMR increasingly start to participate in long-range ion transport also.

For the $Li_xBMIM_{(1-x)}TFSI$ mixtures, in contrast to the EMIMTFSI based systems, the only equilibrium was between a liquid condensed phase of $Li_{x'}BMIM_{(1-x')}TFSI$, being characterized by a high viscosity, and undissolved LiTFSI. Only the phase transitions of LiTFSI were detected (from IIa to Ia and melting of Ia). Even when the samples were stored for four weeks before any measurements had been carried out it was impossible to obtain any crystalline phase corresponding to 1/2 EMIMTFSI/LiTFSI (Ib). The data obtained for $Li_xPY_{13(1-x)}TFSI$ are in very good agreement with those reported in the literature.[5]

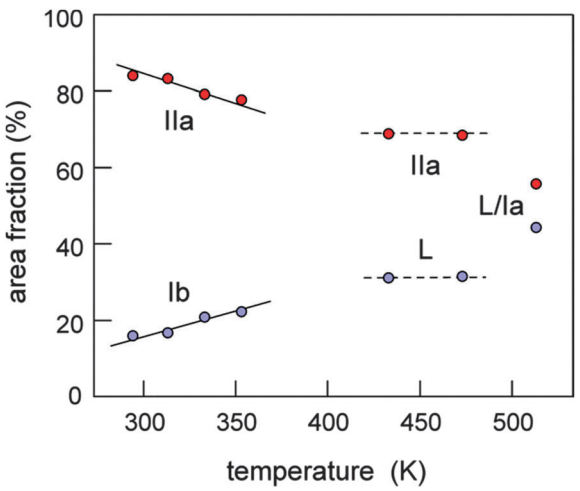

Fig. 4 Area fractions of the two dynamically distinct spin-reservoirs of $Li_xEMIM_{(1-x)}TFSI$ with x = 0.9.

As the thermal behaviour of the materials dramatically depends on the thermal history as well as the composition, the 2nd DSC heating cycle gives a wealth of information. For $x > 0.80$ all the phase transitions; Ib to L, IIa to Ia, and the melting of Ia are all reproducible. In addition, the crystallization during cooling is consistent with the 2nd heating cycle (Fig. 1b). Small heterogeneities of LiTFSI may here act as nucleation centres to facilitate crystallization. For $x < 0.80$,

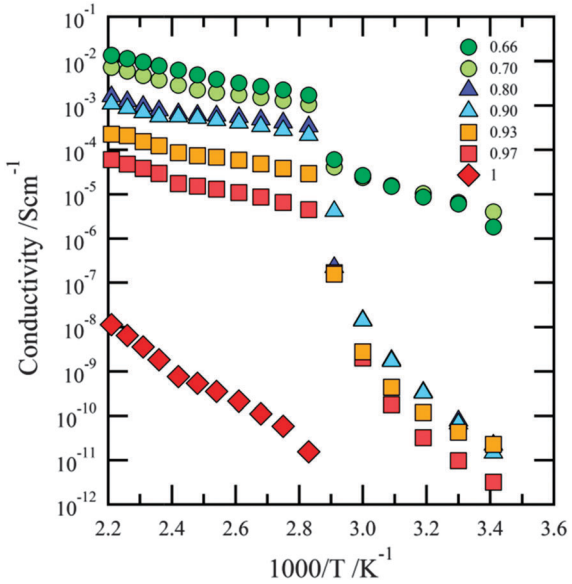

Fig. 5 Ionic conductivities obtained for the $Li_xEMIM_{(1-x)}TFSI$ ($0.66 \leq x \leq 1$) system; data collected during heating.

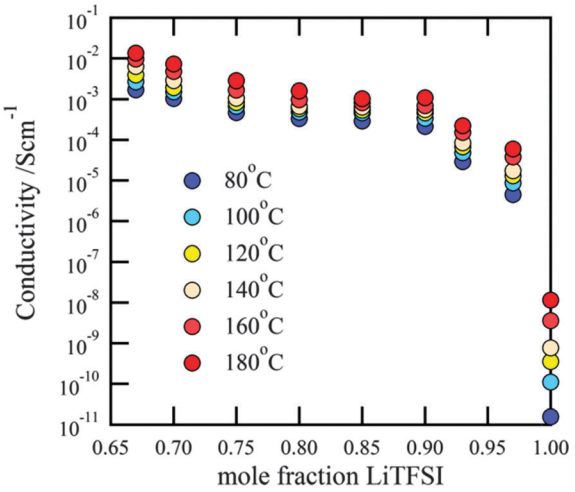

Fig. 6 Conductivity isotherms for the $Li_xEMIM_{(1-x)}TFSI$ ($0.66 \leq x \leq 1$) system as a function of composition; data collected during heating.

the 2nd cycle only records fully amorphous systems, characterized by increasing glass transition temperatures as a function of overall composition x (−32 °C, −25 °C, and −19 °C for x = 0.66, 0.70, and 0.75, respectively). In stark contrast, for x = 0.80 thermal metastability is observed and different amounts of amorphous material have been formed characterized by a T_g of −2 °C. Apart from causing the difference observed in *e.g.* the Ib to L transition temperature, it could also possibly provide different Li ion conductivities. The largest differences for the 2nd heating cycle were observed for the $Li_xPY_{13(1-x)}TFSI$ system for which it was impossible to obtain reproducible results (not shown).

An important distinction to be made is that while the basic thermal behaviour as outlined above is fundamentally promising, the application of long-term high temperature electrochemical cycling using composite electrodes can be highly problematic, which is not investigated here. However, the next section points to the stability of the electrolytes during the high temperature conductivity measurements (with stabilization times of 30 min at each point) and all the materials are also stable during the synthesis procedure with mixing at 250 °C for 1 h.

Ionic conductivity

Moving to a property of crucial importance for an electrolyte, *viz.* ionic conductivity, we observe for all compositions that ion dynamics are strongly correlated with the thermal behaviour of the samples. Previously, this has also been reported for pyrrolidinium (PY) based ILs doped with LiTFSI.[7,16,28] The three regimes being associated with the double phase regions Ib/IIa, L/IIa, and L/Ia, as seen in the DSC data, can also be straightforwardly recognized in the temperature dependent conductivity data (see Fig. 5 and 6).

The region corresponding to the existence of the dual phase Ib/IIa (20 °C to 70 °C) is characterized by very low conductivities ($\sigma \approx 10^{-11}$ S cm^{-1}) which is due to the presence of both crystalline 1 : 2 EMIMTFSI/LiTFSI and crystalline LiTFSI. The only exception is the sample with x = 0.70 ($\sigma \approx 10^{-6}$ S cm^{-1}); very likely, this is due to the presence of some amorphous material. The fact that the ^{7}Li NMR measurements reveal a sharp NMR line even at temperatures as low as room temperature is not in contradiction with the observation of low conductivities: in contrast to DC conductivity which probes long-range motions of the charge carriers, NMR is sensitive to dynamics on much shorter length scales.

Except for the sample with x = 0.7, between 70 °C and 80 °C a rapid increase in conductivity, *viz.* some orders of magnitudes, is observed, which is caused by the melting of the Ib phase. Since this process seem to also affect the ^{7}Li NMR quadrupole powder pattern of the LiTIFSI IIa phase (see Fig. 3a), this phase has potential to also somehow participate in enabling long-range ion transport.

Between 80 °C and 140 °C, that is the L/IIa region, charge carrier transport is characterized by relatively high and stable conductivities with values ranging from 10^{-3} to 10^{-5} S cm^{-1} and with a maximum in conductivity for x = 0.70 ($\sigma \approx 3 \times 10^{-3}$ S cm^{-1}). Only slightly lower conductivities are observed in the compositional range $0.75 \leq x \leq 0.90$ ($\sigma \approx 10^{-4}$ S cm^{-1}). Samples with $x > 0.90$, however, reveal a sudden drop in conductivity. In the last, the third conductivity region, corresponding to L/Ia ($T > 140$ °C), the conductivity increases more rapidly with temperature. Once again, this might indicate that the LiTFSI phase takes part in facilitating ion transport over long distances. Despite the fact that the IIa–Ia phase transition is also detectable for pure LiTFSI in the conductivity measurements, the conductivity of pure LiTFSI is many orders of magnitude lower for the whole T range covered; it increases from 10^{-11} S cm^{-1} at 80 °C to 10^{-8} S cm^{-1} at 180 °C. The highest conductivity values are obtained for samples with x = 0.70 and x = 0.75 ($\sigma \approx 3 \times 10^{-3}$ S cm^{-1}) and are related to the final melting of the crystalline LiTFSI:EMIMTFSI phase Ib which occurs at 138 °C and 151 °C, respectively. Overall, high conductivities are observed for

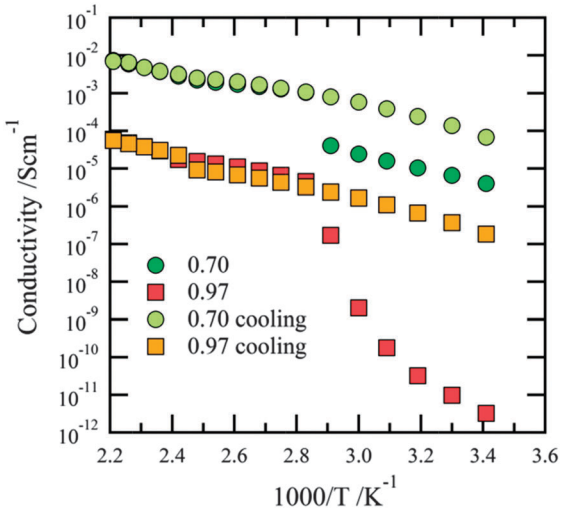

Fig. 7 Comparison of ionic conductivities obtained for the $Li_xEMIM_{(1-x)}TFSI$ (x = 0.70 and x = 0.97) system; data collected during heating and cooling.

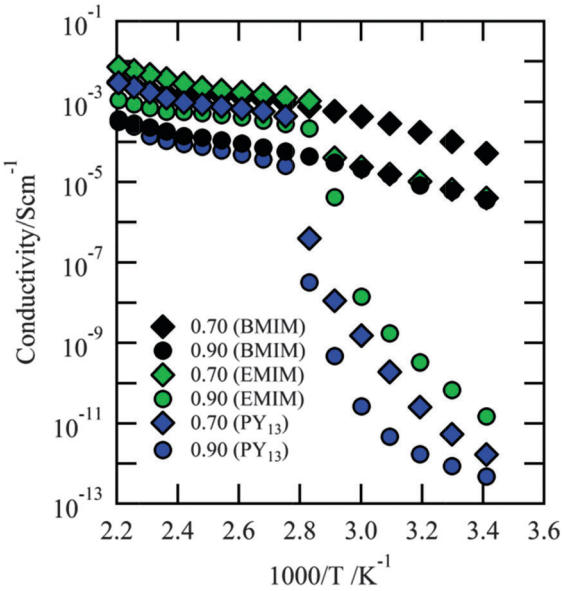

Fig. 8 Comparison of ionic conductivities obtained for the $Li_xEMIM_{(1-x)}TFSI$, $Li_xBMIM_{(1-x)}TFSI$, and $Li_xPY_{13(1-x)}TFSI$ (x = 0.70 and x = 0.90) systems; data collected during heating.

$0.70 < x < 0.90$ and lower conductivities for mixtures with overall compositions of $x > 0.90$.

Most likely, the results from the conductivity measurements and the thermal studies also correlate with the metastability of the different phases (see Fig. 7). Indeed, upon cooling, the Ia to IIa transition is well reproduced, with similar conductivity values as during heating. Similarly, also for the Ib to L transition there is no difference in the slope of the conductivity curves. The latter is in contradiction to the DSC data but can be explained by the tendency to create super-cooled liquid phases (even for $x > 0.80$) and by the fact that the crystallization process is controlled by slow kinetics. Especially the different sizes and shapes of the samples for DSC (few mg, bulk) and conductivity (*ca.* 0.3 g, film) measurements should be taken into account.

A comparison of the temperature dependent ionic conductivity of $Li_xEMIM_{(1-x)}TFSI$, $Li_xBMIM_{(1-x)}TFSI$ and $Li_xPY_{13(1-x)}TFSI$ for the different systems studied (Fig. 8) shows that between 20 °C and 70 °C the highest conductivities are obtained for the BMIMTFSI based samples. This can be explained by the presence of a liquid $Li_{x'}BMIM_{(1-x')}TFSI$ phase rather than a solid–solid dual phase region being characteristic of both the $Li_xEMIM_{(1-x)}TFSI$ and the $Li_xPY_{13(1-x)}TFSI$ systems. The situation changes above 80 °C due to the melting of the Ib phase in the $Li_xEMIM_{(1-x)}TFSI$ system leading to the highest conductivity observed. For x = 0.90 the difference in ionic conductivity between the EMIMTFSI-based system and both the BMIMTFSI and the $PY_{13}TFSI$-based systems is about one order of magnitude above that at 80 °C. While the solvent-in-salt electrolytes can exhibit Li^+ transference numbers as high as 0.73,[14] important for the inhibition of lithium dendrite growth, we have not determined these in this proof-of-concept study – but rely on the robustness of the materials. Further studies should of course properly address this property also. Moving to mechanical properties, the materials are powders at room temperature and easily handled as pellets, but depending on x may turn liquid at the working temperatures aimed at. If the materials will work in a practical cell with respect to issues like electrode wettability is yet an open question calling for experimental evidence.

Adding to practical requirements, an EMIMTFSI-based electrolyte was previously shown to suppress Al current collector corrosion.[29] This was supported more recently when $PY_{14}TFSI$ based electrolytes were also tested up to 60 °C; it was shown that even small amounts of ILs can suppress this phenomenon.[30] In addition, some very recent studies have revealed that by using electrolytes with (very) high concentrations of LiTFSI, even in organic solvents, the normally highly prevalent Al corrosion by TFSI can be hindered.[14,31,32] However, in contrast a very recent study showed that the electrochemical stability of PY_{14}-based electrolytes can be severely reduced at elevated temperatures such as 60 °C, even if TFSI-based ILs performed much better than the corresponding FSI-based ones.[33]

Raman spectroscopy studies

Finally, the macroscopic data for the $Li_xEMIM_{(1-x)}TFSI$ system above are correlated with molecular level Raman spectroscopy data across all compositions and a wide range of temperatures. Raman spectra were collected at 23 °C, 90 °C and 165 °C to investigate the Ib, IIa, Ia, and L phases, respectively. The 735–760 cm^{-1} region of the Raman spectra was chosen in order to obtain information about the anion coordination and thus the nature of the charge carrying species.[16–23]

The pure Ib phase (x = 0.66) is useful as a starting point as the TFSI anion coordination is known[11] and, thus, can serve as an internal reference. Here, the TFSI anion exists in three different combinations of conformation and coordination environment; in two cases in C_1 conformation and either coordinated by three lithium cations by four oxygen atoms or by two lithium cations by three oxygen atoms, and for the remaining case in C_2 conformation and coordinated by two

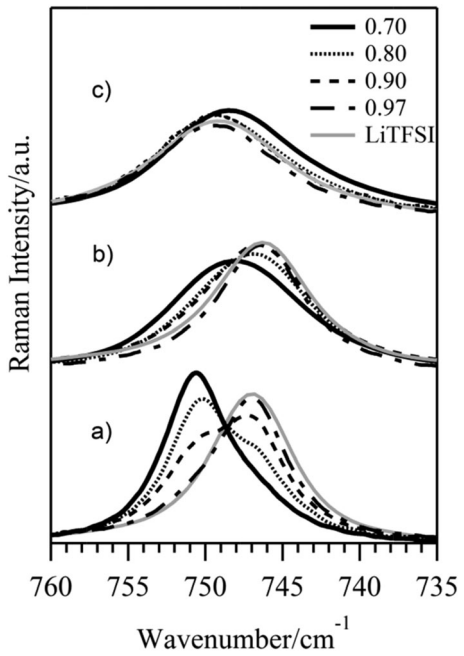

Fig. 9 Raman spectra of the $Li_xEMIM_{(1-x)}TFSI$ ($0.66 \leq x \leq 1$) system; collected at 23 °C (a), 90 °C (b) and 165 °C (c).

lithium cations by three oxygen atoms.[15] Likewise a known structure, in the IIa phase (pure LiTFSI) all TFSI anions are in C_2 conformation and surrounded by four lithium cations each.[25] In general, at room temperature, two bands at *ca.* 747 cm^{-1} and *ca.* 750.5 cm^{-1} are observed for the $Li_xEMIM_{(1-x)}TFSI$ systems (Fig. 9a). The first band can be correlated with the observations for the IIa phase, while the second corresponds to the Ib phase. This is further supported by the observation of an increasing x to continuously decrease the 750.5 cm^{-1} band and increase the 747 cm^{-1} band, until only the latter band remains. The Raman spectra collected at 90 °C (Fig. 9b), corresponding to the IIa/L phases, have wider and down-shifted bands as compared to the spectra collected at 23 °C. For the $x = 0.70$ composition a broad band at 748 cm^{-1} suggests at least two components; with increasing x the band maximum is shifted to 746 cm^{-1}, but with a higher wavenumbers broadening. Adding an analysis of the 260–360 cm^{-1} spectral range (Fig. 10) shows that, besides the bands characteristic of IIa (276 cm^{-1}, 315 cm^{-1}, 330 cm^{-1} and 346 cm^{-1}) a group of signals being characteristic for $[Li(TFSI)_2]^-$ complexes appears upon melting of Ib (282 cm^{-1}, 313 cm^{-1}, 326 cm^{-1}, and a shoulder at 338 cm^{-1}).[22,23] When the temperature is increased further (*i.e.*, up to 165 °C), hence above the IIa to Ia solid–solid phase transition, we observe a wide band located at approximately 749 cm^{-1} for all compositions (Fig. 9c). For $x = 0.70$ the maximum of this band is shifted towards lower wavenumbers by *ca.* 0.8 cm^{-1}. Here, an analysis of the 260–360 cm^{-1} spectral range shows no significant changes for the spectra with $x = 0.70$ (Fig. 10c) *versus* data collected at 90 °C. The largest change occurs for the LiTFSI sample, where the IIa to Ia solid–solid phase transition takes place at 152 °C (Fig. 10c). The Ia phase is characterized by the following bands; 278 cm^{-1} with a shoulder at 284 cm^{-1}, 298 cm^{-1}, 315 cm^{-1} and

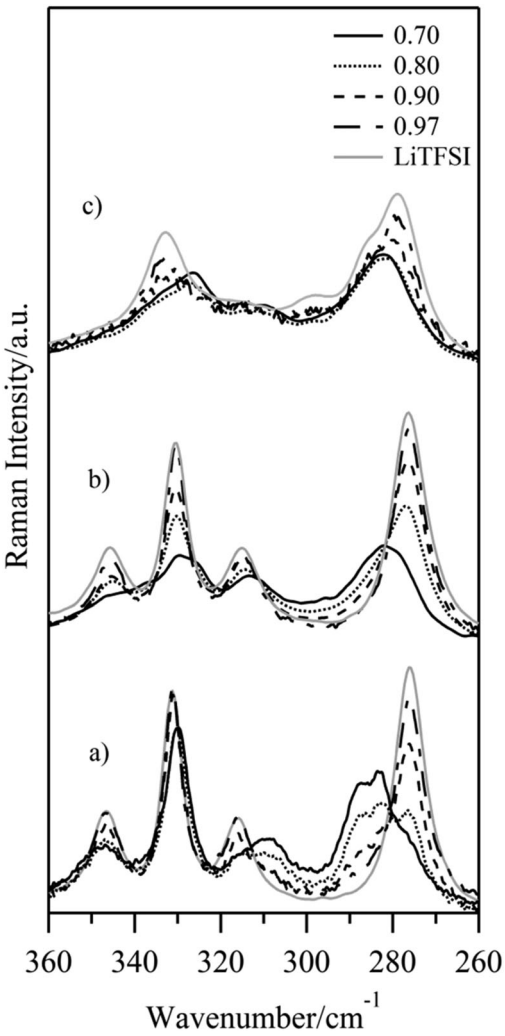

Fig. 10 Raman spectra of the $Li_xEMIM_{(1-x)}TFSI$ ($0.66 \leq x \leq 1$) system; collected at 23 °C (a), 90 °C (b) and 165 °C (c).

335 cm^{-1}. This suggests a change in the conformation state of the TFSI anion in LiTFSI which simultaneously influences the EFG at the site of the ^7Li nucleus, see above.

Considering also literature studies,[17–23] this indicates that the TFSI anion, compared with the pure IIa phase of LiTFSI (746 cm^{-1}) and with the existence in higher agglomerates or polymeric chains (*cf.* the molten Ib phase, 749 cm^{-1}), is also found in $[Li(TFSI)_2]^-$ triplets (746–749 cm^{-1}). The changed TFSI local coordination and charge carrier nature are clearly seen for $x = 0.70$ with a large change in band area ratios upon heating. Indeed, the presence of highly mobile $[Li(TFSI)_2]^-$ can explain the high ionic conductivities observed, albeit rather unexpected for these high x values. As these complexes are largely responsible for the lithium transport in "LiX-in-IL" systems[22,23] the Li^+ cation transport properties can also be arguably similar.

4 Conclusions

To conclude, a conceptually new class of electrolyte materials for high temperature lithium batteries has been studied. The

ionic liquid-in-salt samples studied show promising high ionic conductivities as well as appreciable mechanical strength. Fundamentally, the materials are truly multi-phase and easily super-cooled; they seem to benefit from charge carriers being of the same type as found in classic IL-based electrolytes.

Acknowledgements

M.M. and P.J. are grateful to the Swedish Research Council (VR), the Swedish Research Council for Environment, Agricultural Sciences and Spatial Planning (FORMAS), and Chalmers Energy and Transport Areas of Advance for financial support. M.W. thanks the Austrian Federal Ministry of Economy, Family and Youth, and the Austrian National Foundation for Research, Technology and Development for financial support.

Notes and references

1 J.-M. Tarascon and M. Armand, *Nature*, 2001, **414**, 359.
2 M. Armand, F. Endres, D. R. MacFarlane, H. Ohno and B. Scrosati, *Nat. Mater.*, 2009, **8**, 621.
3 A. Lewandowski and A. Świderska-Mocek, *J. Power Sources*, 2009, **194**, 601.
4 D. R. MacFarlane, J. Huang and M. Forsyth, *Nature*, 1999, **402**, 792.
5 W. A. Henderson and S. Passerini, *Chem. Mater.*, 2004, **16**, 2881.
6 Q. Zhou, W. A. Henderson, G. Appetecchi and S. Passerini, *J. Phys. Chem. C*, 2010, **114**, 6201.
7 M. Forsyth, J. Huang and D. R. MacFarlane, *J. Mater. Chem.*, 2000, **10**, 2259.
8 Q. Zhou, K. Fitzgerald, P. D. Boyle and W. A. Henderson, *Chem. Mater.*, 2010, **22**, 1203.
9 Q. Hu, S. Osswald, R. Daniel, Y. Zhu, S. Wesel, L. Ortiz and D. R. Sadoway, *J. Power Sources*, 2011, **196**, 5604.
10 D. Munoz-Rojas, J.-B. Leriche, C. Delacourt, P. Poizot, M. R. Palacin and J.-M. Tarascon, *Electrochem. Commun.*, 2007, **9**, 708.
11 F. Mestre-Aizpurua, S. Laruelle, S. Grugeon, J.-M. Tarascon and M. R. Palacín, *J. Appl. Electrochem.*, 2010, **40**, 1365.
12 J. Mun, Y. S. Jung, T. Yim, H. H. Y. Lee, H.-J. Kim, Y. G. Kim and S. M. Oh, *J. Power Sources*, 2009, **194**, 1068.
13 C. A. Angell, C. Liu and E. Sanchez, *Nature*, 1993, **362**, 137.
14 L. Suo, Y.-S. Hu, H. Li, M. Armand and L. Chen, *Nat. Commun.*, 2013, **4**, 1481.
15 K. Matsumoto, R. Hagiwara and O. Tamada, *Solid State Sci.*, 2006, **8**, 1103.
16 Q. Zhou, P. D. Boyle, L. Malpezzi, A. Mele, J.-H. Shin, S. Passerini and W. A. Henderson, *Chem. Mater.*, 2011, **23**, 4331.
17 M. Herstedt, M. Smirnov, P. Johansson, M. Chami, J. Grondin, L. Servant and J. C. Lassegues, *J. Raman Spectrosc.*, 2005, **36**, 762.
18 J. C. Lassegues, J. Grondin, R. Holomb and P. Johansson, *J. Raman Spectrosc.*, 2007, **38**, 551.
19 Y. Umebayashi, T. Mitsugi, S. Fukuda, T. Fujimori, K. Fujii, R. Kanzaki, M. Takeuchi and S. Ishiguro, *J. Phys. Chem. B*, 2007, **111**, 13028.
20 L. J. Hardwick, M. Holzapfel, A. Wokaun and P. Novak, *J. Raman Spectrosc.*, 2007, **38**, 110.
21 Y. Umebayashi, S. Mori, K. Fujii, S. Tsuzuki, S. Seki, K. Hayamizu and S. Ishiguro, *J. Phys. Chem. B*, 2010, **114**, 6513.
22 J. C. Lassegues, J. Grondin and D. Talaga, *Phys. Chem. Chem. Phys.*, 2006, **8**, 5629.
23 J. C. Lassegues, J. Grondin, C. Aupetit and P. Johansson, *J. Phys. Chem. A*, 2009, **113**, 305.
24 K. Eichele, *WSolids1 software, version 1.20.21*, Universität Tübingen, 2013.
25 J. L. Nowinski, P. Lightfoot and P. G. Bruce, *J. Mater. Chem.*, 1994, **4**, 1579.
26 A. Abragam, *The Principles of Nuclear Magnetism*, Oxford University Press, 1961.
27 D. Freude, in *Encyclopedia of Analytical Chemistry*, ed. R. A. Meyers, John Wiley & Sons Ltd, Chichester, 2000.
28 W. A. Henderson, S. Passerini, H. C. De Long and P. C. Trulove, *ECS Trans.*, 2008, **11**, 115.
29 B. Garcia and M. Armand, *J. Power Sources*, 2004, **132**, 206.
30 R.-S. Kühnel, M. Lübke, M. Winter, S. Passerini and A. Balducci, *J. Power Sources*, 2012, **214**, 178.
31 K. Matsumoto, K. Inoue, K. Nakahara, R. Yuge, T. Noguchi and K. Utsugi, *J. Power Sources*, 2013, **231**, 234.
32 D. W. McOwen, D. M. Seo, O. Borodin, J. Vatamanu, P. D. Boyle and W. A. Henderson, *Energy Environ. Sci.*, 2014, **7**, 416.
33 R.-S. Kühnel and A. Balducci, *J. Power Sources*, 2014, **249**, 163.